

# Plasma polymerization of allyltrimethylsilane with single-filament dielectric-barrier discharges—Evidence of cationic surface processes

Lars Bröcker<sup>1</sup>  | Tristan Winzer<sup>2</sup> | Nickolas Steppan<sup>1</sup> | Jan Benedikt<sup>2</sup>  | Claus-Peter Klages<sup>1</sup> 

<sup>1</sup>Institute for Surface Technology, IOT, Technische Universität Braunschweig, Braunschweig, Germany

<sup>2</sup>Institute of Experimental and Applied Physics, Faculty of Mathematics and Natural Sciences, Kiel, Germany

## Correspondence

Lars Bröcker, Institute for Surface Technology, IOT, Technische Universität Braunschweig, Riedenkamp 2, Braunschweig 38108, Germany.  
Email: l.broecker@tu-braunschweig.de

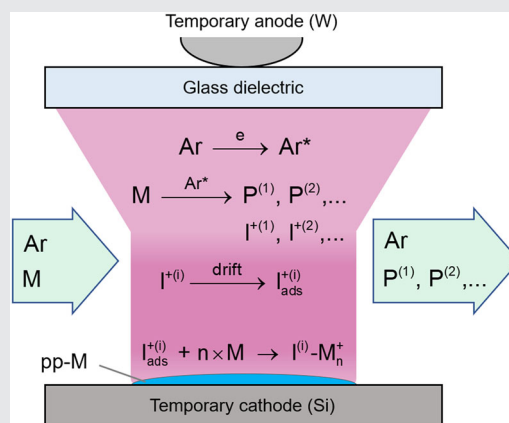
## Funding information

Deutsche Forschungsgemeinschaft

## Abstract

Atmospheric-pressure plasma-enhanced film deposition with single-filament dielectric-barrier discharges (DBDs) in argon was investigated using allyltrimethylsilane (ATMS) as a precursor. Nonionic deposition in the discharge zone is largely precluded by a rapid cross-flow of the source gas, containing between 50 and 2000 ppm of ATMS. The performed experimental studies show a surprisingly large deposited film mass per transferred elementary charge between 220 and 540 amu.

Film growth experiments, mass-spectrometric studies, and kinetic considerations led to the conclusion that the deposition process is a cationic surface polymerization, initiated by ions produced in the DBD by energy transfer from long-lived excited Ar species and propagated by addition of ATMS monomer molecules.



## KEYWORDS

allyltrimethylsilane (ATMS), dielectric-barrier discharge (DBD), ion deposition, plasma polymerization, single filament

## 1 | INTRODUCTION

The investigation of plasma-enhanced chemical vapor deposition from allyltrimethylsilane (ATMS, 3-(trimethylsilyl)-1-propene) at atmospheric pressure,

reported in this article, is motivated by both application-oriented considerations and interest in the deposition mechanism of an unsaturated monomer. The allyl residue of ATMS is expected to open additional chemical reaction pathways such as radical or ionic

This is an open access article under the terms of the [Creative Commons Attribution-NonCommercial-NoDerivs](https://creativecommons.org/licenses/by-nc-nd/4.0/) License, which permits use and distribution in any medium, provided the original work is properly cited, the use is non-commercial and no modifications or adaptations are made.

© 2023 The Authors. *Plasma Processes and Polymers* published by Wiley-VCH GmbH.

addition to the double bond, potentially resulting in changes of the predominant deposition mechanism and in the film properties with the single-filament dielectric-barrier discharge (SF-DBD) setup from Bröcker et al.<sup>[1]</sup>: Plasma polymerization of hexamethyldisiloxane (HMDSO) by means of SF-DBDs in a rapid crossflow of Ar–HMDSO gas mixtures with discharge residence times  $t_{\text{res}}$  of a few ms favors ionic film deposition. At HMDSO fractions  $x_M$  up to about 1000 ppm, the deposition process is largely carried by  $\text{Me}_3\text{SiOSiMe}_2^+$  (penta-methyldisiloxanyl, PMDS<sup>+</sup>) ions, while gas-phase oligomerization eventually sets in at larger monomer fractions. Incorporation of monomer molecules into the deposit by reactions with surface free radicals, is only enabled by the presence of double bonds in a monomer carrying, for example, a vinyl or allyl substituent. Besides the investigation of the polymerization process, the chemical structure and mechanical properties of plasma polymers obtained from unsaturated monomers are of interest, too, due to a potentially higher degree of cross-linking.

Table 1 lists the ionization energies,  $IE$ , of the oxygen-free organosilanes tetramethylsilane (TMS), vinyltrimethylsilane, (trimethylsilyl)-ethene), ATMS, and hexamethyldisilane (HMDS) that are currently investigated in the SF-DBD setup:

Among the monosilanes in the first three columns, ATMS plays a distinct role due to the so-called  $\beta$ -silicon (or beta-silicon) effect, that is, hyperconjugation (or  $\sigma$ - $\pi$  conjugation) between the Si–C bond, connecting the trimethylsilyl residue to the propene unit, and the  $\pi$  system of  $-\text{CH}=\text{CH}_2$ . A direct consequence of this effect is a comparably small ionization energy of ATMS, which is related to the increased energy of the highest occupied molecular orbital, see Table 1.<sup>[3]</sup>

Ionization of ATMS by collisions with electrons of several tens of eV energy in a conventional mass spectrometer results in fragmentation of the primary product, the radical cation  $\text{ATMS}^{+\bullet} = [\text{Me}_3\text{SiCH}_2\text{CHCH}_2]^{+\bullet}$ , into a resonance-stabilized allyl radical and a trimethylsilyl cation  $\text{Me}_3\text{Si}^+$  (73 amu).<sup>[5]</sup> Chiavarino et al. studied the reactions of collisionally stabilized  $\text{ATMS}^{+\bullet}$  with added neutrals, acting as bases and nucleophiles, respectively. Depending on the type of the reaction partner,  $\text{ATMS}^{+\bullet}$  transfers either  $\text{H}^+$  or  $\text{Me}_3\text{Si}^+$ .<sup>[6]</sup> ATMS was also utilized as a

source of  $\text{Me}_3\text{Si}^+$  for desorption chemical ionization mass spectroscopy.<sup>[7]</sup> Here, products of the addition of  $\text{H}^+$ ,  $\text{Me}_3\text{Si}^+$ , as well as of the allyldimethylsilyl cation ( $\text{ADMS}^+$ , 99 amu) to the parent compound were observed, with masses of 115, 187, and 213 amu for  $[\text{ATMS} + \text{H}]^+$ ,  $[\text{ATMS} + \text{Me}_3\text{Si}]^+$ , and  $[\text{ATMS} + \text{ADMS}]^+$ , respectively.<sup>[7]</sup> Only for the 115 amu cation, a reaction with another ATMS molecule was observed with low intensity, forming  $[\text{ATMS} + \text{H} + \text{ATMS}]^+$  with 229 amu. The authors described these adducts as “not highly reactive,” as further addition reactions of these ions to ATMS apparently did not take place. Note that the ions obtained by addition of  $\text{Me}_3\text{Si}^+$  or  $\text{ADMS}^+$  to ATMS are doubly stabilized by the  $\beta$ -silicon effect.

In view of these reports, it was surprising to find that the deposition of plasma-polymerized ATMS (pp-ATMS) under conditions of the SF-DBD results in the formation of a deposited film mass per Faraday of transferred charge, in the following abbreviated by the symbol  $m_q$ , up to 540 g/mol. In these experiments, the ATMS “monomer” (M) is highly diluted by argon and predominantly ionized by long-lived excited argon species  $\text{Ar}^*$ , where  $\text{Ar}^*$  is the collective name for Ar atoms in metastable ( $1s_5$  and  $1s_3$ ) or resonant ( $1s_4$  and  $1s_2$ ) states with excitation energies between 11.55 and 11.83 eV,<sup>[8]</sup> as well as excited argon dimers (excimers),  $\text{Ar}_2(^3\Sigma_u^+)$  with 9.8 eV.<sup>[9]</sup> With an  $IE$  of 9.0 eV, ATMS can be ionized by energy transfer from any of the  $\text{Ar}^*$  species. The combination of low excess energy of the ionizing species with a high Ar gas pressure guarantees that the primary product  $\text{ATMS}^{+\bullet}$  is effectively stabilized against unimolecular fragmentations.

The focus of the present publication is on the presentation and discussion of experimental results obtained with a range of molar monomer fractions  $x_M$  between 50 and 2000 ppm. For  $x_M = 1000$  ppm, the effect of several important process parameters—substrate temperature, gas-flow velocity, excitation frequency, and—in the case of pulsed plasma excitation—pulse and pause lengths were investigated, in order to enable conclusions regarding the deposition mechanism. Besides the thin film diagnostics and electrical characterization of the plasma, mass spectrometry measurements of positive ions were performed in a DBD reactor with the same discharge geometry like the setup used for deposition experiments.

TABLE 1 Abbreviated names, structures, and ionization energies,  $IE$ , of selected organosilanes,  $\text{Me} = \text{CH}_3$ .

TMS	VTMS	ATMS	HMDS
$\text{Me}_3\text{Si}-\text{Me}$	$\text{Me}_3\text{Si}-\text{CH}=\text{CH}_2$	$\text{Me}_3\text{Si}-\text{CH}_2-\text{CH}=\text{CH}_2$	$\text{Me}_3\text{Si}-\text{SiMe}_3$
9.8 eV <sup>[2]</sup>	9.8 eV <sup>[3]</sup>	9.0 eV <sup>[3]</sup>	8.27 eV <sup>[4]</sup>

Abbreviations: ATMS, allyltrimethylsilane; HMDS, hexamethyldisilane; TMS, tetramethylsilane; VTMS, vinyltrimethylsilane.

## 2 | EXPERIMENTAL SECTION

### 2.1 | Materials

ATMS (98%) was obtained from abcr GmbH. Argon (purity 6.0) was purchased from Linde AG. Dried acetone with a maximum water content of 75 ppm and p-xylene (99%) were obtained from Merck KGaA. Silicon wafers of 500  $\mu\text{m}$  thickness with a resistivity of 10–20  $\Omega\text{cm}$  were obtained from SIEGERT WAFER GmbH.

### 2.2 | Instrumentation

Plasma polymerization experiments were performed at atmospheric pressure with a single-filament DBD reactor having an asymmetric electrode arrangement: A tungsten tip served as the high-voltage electrode and an aluminum plate as the ground. Silicon wafer pieces ( $1.0 \times 2.2 \text{ cm}^2$ ) were cleaned with acetone and placed on the ground as substrates. The dielectric barrier was a 1.1-mm thick glass plate from Borofloat 33, and the tungsten tip was glued onto the dielectric using epoxy resin (RS Pro Quick Set Epoxy Adhesive) from RS Components Ltd. For more details of the DBD reactor as well as the electrical circuit used to measure the dissipated energy, the discharge current, and the transferred charge, see a previous publication.<sup>[1]</sup>

The deposited film volume  $V_p$  was obtained by numerical integration of thickness distributions  $d(r)$  measured profilometrically with a *Dektak XT* (Bruker). Scans were performed through the center of the circular-symmetric deposits in gas flow direction and across with a stylus force of 3 mg and a scan time of 30 s; for more information, see Bröcker et al.<sup>[1]</sup> The elemental film composition was measured by wavelength-dispersive X-ray spectroscopy (WDXS) with 5 keV electron energy at three spots close to the center of the deposits, separated by about 20  $\mu\text{m}$ , using a *Cameca SX50* (Cameca). For fourier-transform infrared in attenuated total reflexion (FTIR-ATR) analysis, a *Spotlight 200i FTIR Microscopy System* (Perkin Elmer) was used, equipped with a germanium ATR crystal. The average angle of incidence was 38° and the aperture was 50  $\times$  50  $\mu\text{m}^2$ . A total of 512 scans were accumulated at a spectral resolution of 4  $\text{cm}^{-1}$ . ATR correction was done with the *OMNIC* software by Thermo Fisher Scientific, using a refractive index of the plasma polymer of  $n_{pp} = 1.5$ . This choice is justified by the absence of interference colors of deposits on polyethylene substrates. Therefore, one can conclude that, within an error range of  $\pm 0.05$ , the deposits have the same refractive index like polyethylene ( $n_{PE} = 1.5^{[10]}$ ). Raman measurements were performed

using a *DXR2 Raman Microscope* (Thermo Fisher Scientific) with a laser wavelength of 532 nm, a laser power of 0.5 mW, and a 25- $\mu\text{m}$  monochromator slit. Fifty exposures of 5 s length were accumulated for every spectrum.

Mass spectrometry measurements were performed using a quadrupole mass spectrometer (HIDEN EQP-6 with a mass range up to 510 amu) and a two-stage differential pumping system for sampling of ions from atmospheric pressure. Both stages were pumped down by turbo molecular pumps (Pfeiffer Vacuum). Ions enter the first stage through a grounded 20  $\mu\text{m}$  platinum orifice (Plano EM) and are focused by a system consisting of four electrostatic lenses into the 1-mm orifice connecting the two stages. More details on the setup and tuning of the electrostatic lens system can be found in Große-Kreul et al.<sup>[11]</sup> The 20- $\mu\text{m}$  orifice is an integral part of the CF-100 top flange of the mass spectrometry setup, providing a flat horizontal surface for connecting different types of discharge reactors. Typical pressures in the setup are around  $10^{-2}$  Pa in the first stage and  $5 \times 10^{-5}$  Pa in the second stage, housing the mass spectrometer. The reactor setup from Große-Kreul et al.<sup>[1]</sup> was modified so that the plasma can be ignited directly on the grounded orifice: Besides the absence of the bottom of the reactor, no substrate is needed for mass spectrometric investigations. For this publication, the DBD arrangement was mounted in such a way that the center of the plasma and hence the center of the deposit are located approximately 0.5 mm behind the orifice in gas flow direction and 1.0 and 1.5 mm to the right, respectively. Figure 1a shows schematically the cross section of the orifice with the photograph of a discharge ignited under the conditions reported in Section 2.3, with 100 ppm ATMS in argon. Additionally, Figure 1b indicates the positions of the orifice relative to a thin film with a central thickness of 4  $\mu\text{m}$ , deposited with 100 ppm ATMS.

It is important to note that for mass spectrometric investigations, the ATMS fraction as well as the position of the orifice to the center of the plasma was varied. Two exemplary spectra for 100 and 2000 ppm ATMS, respectively, are shown in this publication as measured at 1.0 and 1.5 mm distance from the symmetry axis. Sampling positions are chosen in the range between 1.0 and 1.5 mm from the symmetry axis (see Figure 1b) due to two reasons: If the orifice is too far away from the first interference ring of the deposit, the formed ions are most likely only products of photoionization by radiation from the plasma. Ions produced in the discharge are not detected. However, if the orifice is too close to the center of the discharge, (i) the deposition rate is too high and the plasma polymer seals the orifice within seconds and (ii) filaments are repeatedly ignited on the edge of the orifice and very high signals of argon ions occur. This can

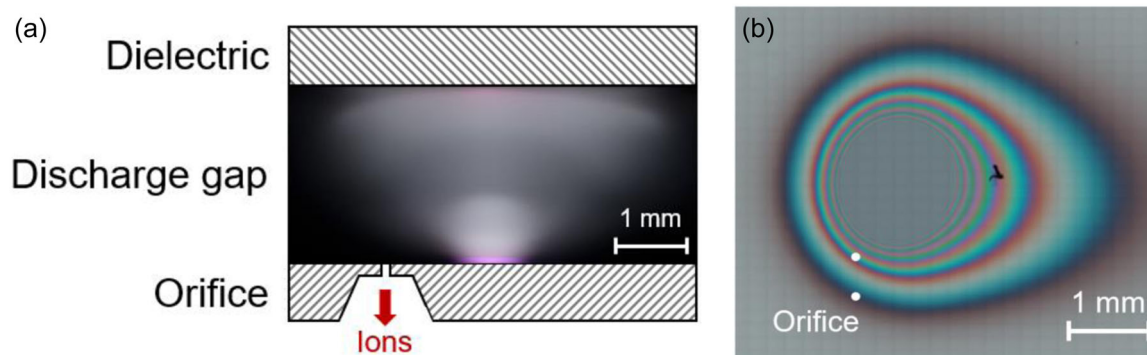


**FIGURE 1** (a) Schematic front view of the cross section where the orifice is positioned in relation to the location of the discharge for 100 ppm allyltrimethylsilane (ATMS) in argon. (b) Microscope image of a thin film deposited from 100 ppm ATMS in argon with a central thickness of  $4\ \mu\text{m}$ , positions of the orifice.

even lead to a partial ablation of the polymer film and, therefore, to an increased detection of ionized fragments. Additionally, the fast clogging of the sampling orifice does not allow to perform any tuning of the mass spectrometer on the ions generated in the plasma. Especially the mass range above 250 amu could not be optimized, where the mass sensitivity is already reduced due to its typical scaling with  $(m/z)^{-1}$ .

### 2.3 | Procedures

Standard conditions for film deposition experiments were as follows: An argon gas flow velocity of 50 cm/s, ATMS molar fractions in the range of  $50\ \text{ppm} \leq x_M \leq 2000\ \text{ppm}$ , continuous-wave (cw) excitation at a frequency of 19 kHz, and an applied operating voltage amplitude  $U_{a0} = 1.75 \pm 0.05\ \text{kV}$ . For a fixed ATMS concentration of 1000 ppm, the effects of the following parameter variations were studied: (1) pulsed plasma excitation with pulse/pause ratios of 1:4 (60:240  $\mu\text{s}$ ) and 1:8 (60:480  $\mu\text{s}$ ) with the same total plasma on-time as for the experiments in cw mode; (2) frequencies of 10, 28, and 44 kHz; (3) a gas flow velocity of 200 cm/s; and (4) substrate temperatures of 70°C and 100°C. For the latter experiments, the reactor was placed on a heating plate.

Extinction voltages  $U_{a0,ex}$  were determined as a function of the admixed monomer fraction: The applied voltage was increased until the plasma was ignited and then decreased again to the point where the voltage signal from the capacitor was no longer visible on the oscilloscope. The voltage at which the discharge disappears is the extinction voltage. For determining the deposition times required to get particular values of the deposits' central thicknesses  $d(0)$ , deposits were first made with deposition times as used for HMDSO; see the previous paper.<sup>[1]</sup> These deposits with  $2\ \mu\text{m} \leq d(0) \leq 4\ \mu\text{m}$

were used for profilometric measurements. Regarding FTIR-ATR, Raman, and WDXS measurements, deposition times were adjusted to obtain thin films with a central thickness of  $4\ \mu\text{m}$ . Before each experiment, the reactor was purged for 5 min with a gas stream mixed from 80 sccm argon bubbled through ATMS at 20°C and diluted by 2 slm pure argon. After film deposition, analyses of the samples were performed within 8 h.

To investigate the solubility and swelling behavior of the deposits, samples coated with admixtures of 1500 and 2000 ppm ATMS, respectively, were stored for 1 h in room-temperature acetone and in hot xylene (100°C), respectively.

Mass spectrometric measurements were performed with the standard plasma parameters given above. Tuning of the mass spectrometer and the electrostatic lens system was performed using a photoionization source and HMDS as a precursor because the HMDS monomer ion possesses a mass of 146 amu and is approximately in the middle of the mass region of interest up to 400 amu. The photoionization source provided significantly lower film deposition rates than those of the SF-DBD, so optimizing the mass spectrometer and ion lens settings over a time period of hours becomes possible without clogging the 20- $\mu\text{m}$  orifice. As expected, high ion fluxes were generated in the SF-DBD, and the electrostatic lens system was slightly detuned in the last step to reduce the total ion flux into the mass spectrometer and protect the secondary electron multiplier detector. Due to measurement time limitations because of the high deposition rate of the SF-DBD, mass spectra were taken only for a single ion energy and in steps of 0.25 amu with a measurement time of 25 ms per step. This led to a measurement time of approximately 40 s per mass spectrum from 10 to 400 amu. At the chosen ion energy, the signal of the HMDS monomer ion is the highest. Because the gas mixture is mainly

composed from Ar, the sampled ions will all have terminal velocity gained in the supersonic expansion behind the sampling orifice being equal to the terminal argon velocity (seeding effect). Therefore, all ions will have slightly different energy scaling linearly with the ion mass. Measuring at a fixed ion energy optimized for the mass of 146 amu can result in possible discrimination of lighter and heavier ions as discussed in Große-Kreul et al.<sup>[11]</sup>

### 3 | RESULTS

#### 3.1 | Extinction voltages

Upon slowly decreasing the applied voltage  $U_{a0}$ , the discharge extinguishes when  $U_{a0}$  reaches the “extinction voltage,”  $U_{a0,ex}$ . A rapid decline of the extinction voltage for small monomer fractions ( $x_M \leq 500$  ppm) is a good indicator that Penning ionization is of relevance under the investigated conditions, see Bröcker et al.<sup>[1]</sup> Figure 2 shows the values of  $U_{a0,ex}$  measured for mixtures of Ar with HMDSO and ATMS, respectively, as a function of the monomer fractions from  $x_M = 10$  to 2750 ppm, as well as the applied voltage used in film deposition experiments. For pure argon, the plasma extinguishes at 3.6 kV. Due to limitations of the experimental setup, no reliable measurements were possible with ATMS fractions below 25 ppm.

Both argon/monomer mixtures are characterized by a strong decline of  $U_{a0,ex}$  with  $x_M$  increasing up to approximately 250–300 ppm.  $U_{a0,ex}$  passes a minimum of 1.1 kV for HMDSO and 1.0 kV for ATMS, and then increases slowly up to the maximum studied molar fraction,  $x_M = 2750$  ppm. For a given  $x_M$ , extinction voltages of discharges in Ar/ATMS mixtures are always smaller than those in Ar/HMDSO, enabling deposition of thin films at 1.75 kV even for  $x_M \geq 3000$  ppm.

Diagrams of the dissipated energy and discharge currents  $i_p(t)$  as a function of  $x_M$  are very similar to the corresponding diagrams already published for Ar/HMDSO mixtures, see Bröcker et al.<sup>[1]</sup> and are, therefore, not shown here.

#### 3.2 | Film volumes per transferred charge

Thin film volumes  $V_p$  were obtained by numerical integration of profilometric line scans in gas flow direction and perpendicular to it, as mentioned in Section 2.2.

Figure 3 shows  $V_p$  and the charge  $q_t$  transferred per period to the silicon wafer as a function of the ATMS

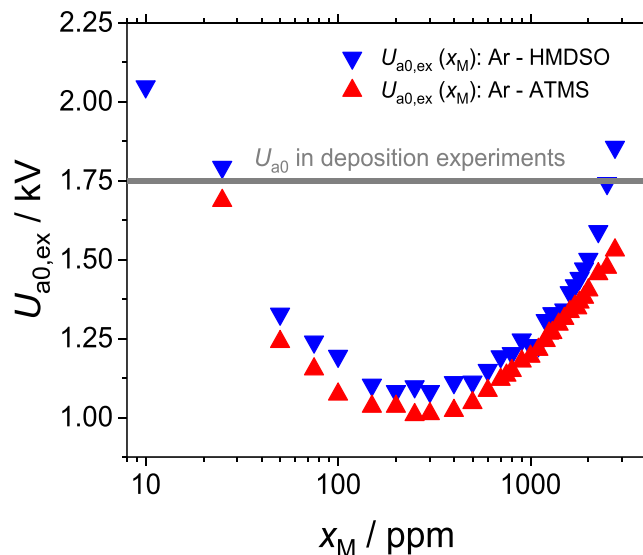


FIGURE 2 Extinction voltages as functions of the molar fraction  $x_M$ , for 10–2750 ppm hexamethyldisiloxane (HMDSO) in argon and 25 to 2750 ppm allyltrimethylsilane (ATMS) in argon, respectively.

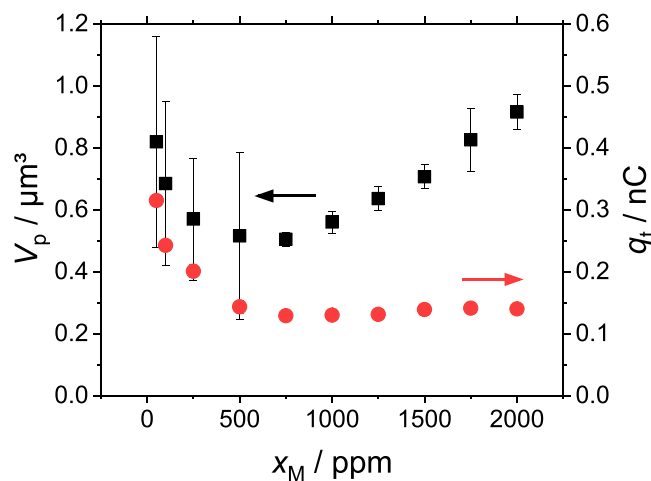
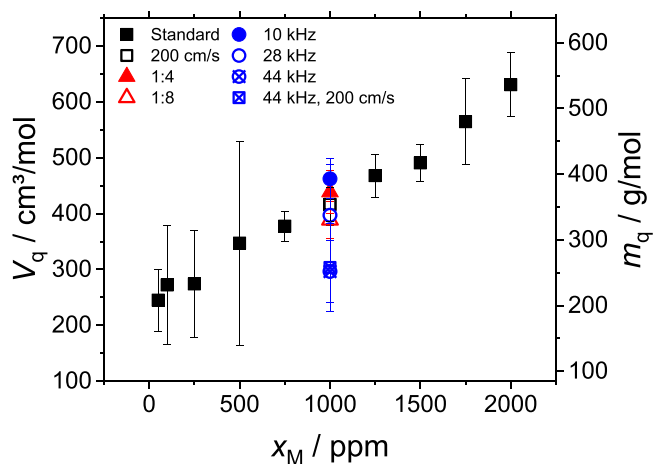


FIGURE 3 Profilometric volume  $V_p$  in  $\mu\text{m}^3$  and transferred charge  $q_t$  in nC for allyltrimethylsilane fractions from 50 to 2000 ppm.

admixture. It is visible that the profilometric volume and the transferred charge follow the same declining trend up to approximately 750 ppm. This decrease correlates with a general decrease of the dissipated energy in the plasma. For growing  $x_M$ , both curves diverge: Whereas  $q_t$  remains nearly constant with a value of 0.14 nC,  $V_p$  increases from a minimum of  $0.5 \mu\text{m}^3$  at 750 ppm to  $0.92 \mu\text{m}^3$  for 2000 ppm.

Calculations of  $V_p$  for 1000 ppm ATMS at elevated substrate temperatures of  $70^\circ\text{C}$  and  $110^\circ\text{C}$  result in values of  $0.52 \pm 0.004$  and  $0.46 \pm 0.046 \mu\text{m}^3$ , respectively,



**FIGURE 4** Volumes per charge  $V_q$  for allyltrimethylsilane fractions between 50 and 2000 ppm. Standard parameters (full black squares): cw, 19 kHz, 50 cm/s. For experiments with parameter variations (open squares, colored symbols), see the legend.

in comparison with  $0.56 \pm 0.036 \mu\text{m}^3$  from Figure 3. A measurement of the transferred charge for increased temperatures was not successful, but a change of the visual appearance of the plasma was not visible. The comparatively small influence of the substrate temperature on the deposition process is discussed in Section 4.3.1.

By dividing  $V_p$  by the transferred charge and multiplying with the Faraday constant  $F$ , the volume per Faraday of transferred charge  $V_q$  is calculated. This is shown in Figure 4 as black squares (“Standard” experiments). For a monomer fraction of 1000 ppm, experiments with pulse/pause ratios of 1:4 (60:240  $\mu\text{s}$ ) and 1:8 (60:480  $\mu\text{s}$ ) but the same overall plasma on-time were done to investigate whether film deposition takes place during plasma off-times. Additionally, the frequency was varied (10, 28, and 44 kHz) and an elevated gas flow velocity of 200 cm/s (also for 44 kHz) was investigated.

For experiments with continuous-wave mode,  $V_q$  increases virtually linearly from 250  $\text{cm}^3/\text{mol}$  at 50 ppm to 630  $\text{cm}^3/\text{mol}$  at 2000 ppm ATMS in argon. The linear and generally increasing trend suggests some kind of polymerization process, see the discussion for a more detailed analysis. An increase of the gas flow velocity to 200 cm/s has no effect on the deposited volume per charge. Elevated pause times have no clear influence on the volume per charge, too, indicating that no thin film deposition takes place during plasma off-times. Interestingly, the frequency seems to influence  $V_q$ : A decrease of  $V_q$  is observed when the frequency is increased from 10 to 44 kHz. Elevated gas flow velocities of 200 cm/s

**TABLE 2** Profilometric volume  $V_p$ , transferred charge  $q_t$ , volume per Faraday of transferred charge  $V_q$ , and mass per Faraday of transferred charge  $m_q$  for experiments performed with 1000 ppm ATMS in argon.

Varied parameter	$V_p$ ( $\mu\text{m}^3$ )	$q_t$ (nC)	$V_q$ ( $\text{cm}^3/\text{mol}$ )	$m_q$ (g/mol)
(Standard parameters)	0.56	0.13	427	382
$\vartheta = 70^\circ\text{C}$	0.52	-	-	-
$\vartheta = 110^\circ\text{C}$	0.46	-	-	-
$v = 200$ cm/s	0.55	0.13	417	373
Pulse/pause: 1:4 (60:240 $\mu\text{s}$ )	0.86	0.19	438	392
Pulse/pause: 1:8 (60:480 $\mu\text{s}$ )	0.64	0.16	388	348
$f = 10$ kHz	0.69	0.15	462	413
$f = 28$ kHz	0.63	0.15	397	355
$f = 44$ kHz	0.85	0.28	296	265
$f = 44$ kHz, $v = 200$ cm/s	1.05	0.33	303	272

Note: Standard parameters: cw, 19 kHz, 50 cm/s, 25°C.

Abbreviation: ATMS, allyltrimethylsilane.

have again no influence on  $V_q$  at 44 kHz, similar to experiments in cw mode.

The film mass deposited per Faraday of transferred charge  $m_q$  is calculated by dividing  $V_q$  through the density  $\rho$  of the plasma polymer and is shown on the right axis of Figure 4. Due to the small dimensions of the deposits, an experimental determination of their density is currently not possible. Therefore, the assumption was made that  $\rho$  equals the mass density of poly(allyltrimethylsilane), 0.895  $\text{g}/\text{cm}^3$ , as quoted by Murahashi et al. for polymers obtained with Ziegler catalysts.<sup>[12]</sup>

In addition to the graphical representation of results in Figure 4, Table 2 shows numerical values of the profilometric volume  $V_p$ , the transferred charge  $q_t$ , as well as  $V_q$  and  $m_q$ , for experiments performed with 1000 ppm ATMS in argon.

### 3.3 | WDXS analysis

Heavy-atom (Si, C, O) contents of the plasma polymers are helpful to gain knowledge of the deposited species. They were obtained by WDXS analysis 4 h after deposition for films obtained from ATMS with  $50 \leq x_M \leq 2000$  ppm. Figure 5 shows atom number ratios  $[\text{C}]/[\text{Si}]$  and  $[\text{O}]/[\text{Si}]$  in this range of ATMS molar fractions.

After a relatively strong decrease of  $[C]/[Si]$  and  $[O]/[Si]$  with increasing  $x_M$  from 50 to 100 ppm, the atom number ratios decline much more slowly for a further growth in  $x_M$ . Whereas the  $[C]/[Si]$  ratio decreases from 5.1 to 4.7 between 100 and 2000 ppm, the  $[O]/[Si]$  ratio declines from 0.32 to 0.25. The oxygen fraction  $[O]/[Si+C+O]$  is below 6.5% for  $x_M \leq 250$  ppm and below 5% beyond 250 ppm. Furthermore, the carbon content  $[C]/[Si+C+O]$  varies only slightly between 78% and 80% over the whole  $x_M$  range. The  $[C]/[Si]$  ratio is a useful parameter to discuss possible film-forming species, see Section 4.4.

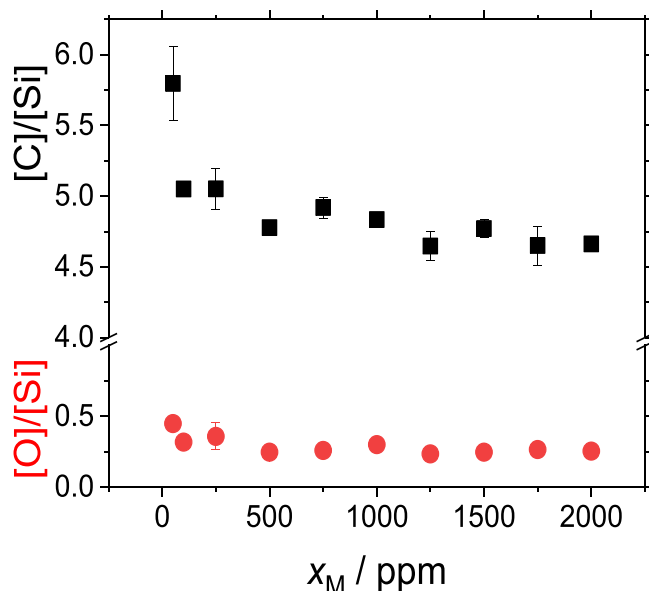


FIGURE 5 Atom number ratios  $[C]/[Si]$  and  $[O]/[Si]$  for plasma polymers from allyltrimethylsilane for monomer fractions between 50 and 2000 ppm.

### 3.4 | FTIR and Raman measurements

The deposited films are insoluble in organic solvents: Film thickness and volumes do not change measurably upon 1-h exposition to room-temperature acetone or 100-°C hot xylene, indicating a high degree of cross-linking. For this reason and due to the small deposited mass of typically a few  $\mu\text{g}$ , the application of powerful analytical methods such as nuclear magnetic resonance spectroscopy is excluded and only vibrational-spectroscopic methods will be used to shed some light on the molecular structure of the deposits. Figure 6 shows an FTIR-ATR spectrum of a plasma polymer deposited with an ATMS fraction of 1000 ppm. All deposits obtained at  $x_M > 250$  ppm (with oxygen fraction below 5%, see Section 3.3) have nearly identical spectra. The virtual absence of structural changes, while the deposited volume per charge nearly doubles between  $x_M = 500$  and 2000 ppm, indicates that the film deposition involves some kind of polymerization. Table 3 lists every peak position obtained in a wavelength interval of 600 up to  $4000\text{ cm}^{-1}$ , the assigned moieties, as well as the associated literature. Whereas “I” indicates that a particular band was visible in the IR, “R” means it was visible in the Raman spectra.

An important observation regarding Figure 6, see the dashed red lines, is the absence or only very weak appearance of bands attributable to vibrations of the allyl group: The typical sharp and large bands of the  $=C-H$  stretch at  $3080\text{ cm}^{-1}$ <sup>[16]</sup> and of the  $C=C$  stretch at  $1640\text{ cm}^{-1}$ <sup>[13]</sup> are absent, whereas the  $C=C$  twist at  $1000\text{--}990\text{ cm}^{-1}$ <sup>[13]</sup> and the wagging vibrations for  $=CH_2$  between  $920$  and  $880\text{ cm}^{-1}$ <sup>[13]</sup> are difficult to investigate due to overlapping with bands from the plasma polymer. It is worth mentioning that a broad and weakly absorbing

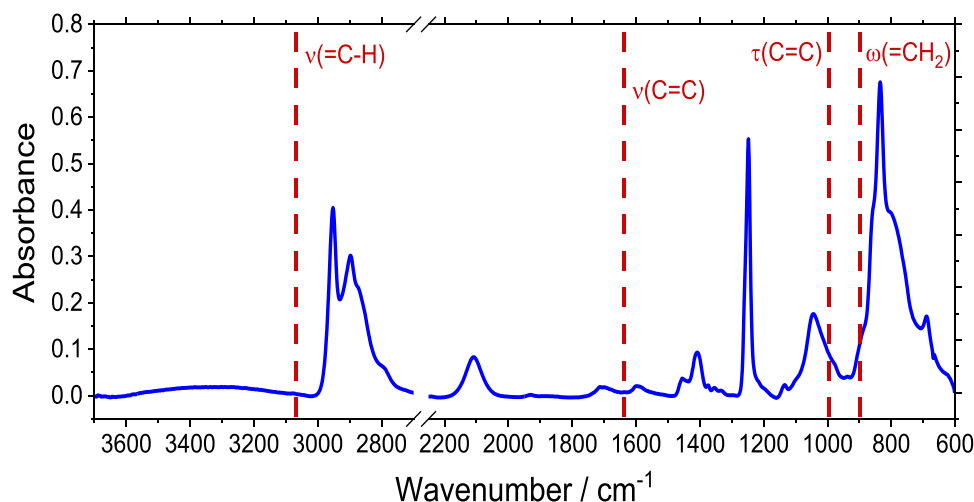


FIGURE 6 FTIR-ATR spectrum of a deposit from 1000 ppm allyltrimethylsilane. The spectrum was ATR and baseline corrected. Peaks are shown in the  $3700\text{--}600\text{ cm}^{-1}$  wavenumber interval. The red dashed lines show peak positions of the allyl group.

**TABLE 3** FTIR and Raman peak positions, assignments, and literature data.

$\nu$ (cm <sup>-1</sup> )	Assignment	Literature
3395–3260 (I)	(OH) hydrogen bonded in Si-OH (OH) hydrogen bonded in C-OH	3400–3200 <sup>[13]</sup> 3550–3230 <sup>[14]</sup>
2954–2952 (I, R)	(CH <sub>3</sub> ) in SiMex	2970 <sup>[13]</sup>
2900–2898 (I, R)	(CH <sub>3</sub> ) in SiMex	2910 <sup>[13]</sup>
2112–2108 (I, R)	(SiHx)	2250–2100 <sup>[14]</sup>
1930 (I)	Si-CH=CH <sub>2</sub> overtone	1950–1900 <sup>[13]</sup>
1714–1699 (I)	(C=O)	1745–1715 <sup>[13]</sup>
1599–1587 (I, R)	(C=C) in alkenyls	1610–1590 <sup>[13]</sup>
1456 (I, R)	(CH <sub>3</sub> ) aliphatic and/or (CH <sub>2</sub> ) aliphatic	1465–1440 <sup>[14]</sup> 1480–1440 <sup>[14]</sup>
1407 (I, R)	(CH <sub>3</sub> ) in SiMex	1440–1390 <sup>[13]</sup>
1375–1373 (I)	(CH <sub>3</sub> ) aliphatic	1375 <sup>[13]</sup>
1353 (I)	(CH <sub>2</sub> ) in Si-CH <sub>2</sub> -Si	1380–1340 <sup>[13]</sup>
1333 (I)	(CH) aliphatic	1360–1320 <sup>[14]</sup>
1250–1248 (I, R)	(CH <sub>3</sub> ) in SiMex	1280–1240 <sup>[13]</sup>
1134–1133 (I)	(CH <sub>2</sub> ) in allyls	1190–1140 <sup>[13]</sup>
1066–1062 (I)	(Si-O-Si)	1130–1000 <sup>[13]</sup>
1045 (I)	(Si-CH <sub>2</sub> -Si)	1080–1040 <sup>[13]</sup>
1026–1024 (I)	(Si-O-Si)	1130–1000 <sup>[13]</sup>
937 (I)	(=CH <sub>2</sub> ) in alkenyls	980–940 <sup>[13]</sup>
835 (I, R)	(Si-C), (CH <sub>3</sub> ) in SiMe <sub>3</sub>	845 <sup>[13]</sup>
803 (I)	(Si-C), (CH <sub>3</sub> ) in SiMe <sub>2</sub>	805 <sup>[13]</sup>
690–688 (I, R)	(Si-C)	684 <sup>[15]</sup>
606 (R)	(Si-C)	618 <sup>[15]</sup>

band of C=C stretching vibrations of alkenyls can always be seen between 1599 and 1587 cm<sup>-1</sup>. Due to the absence of the allyl assignments at 3080 and 1640 cm<sup>-1</sup>, most likely vinyl or other alkenyls are present in the plasma polymers. Furthermore, the wagging vibrations of -CH<sub>2</sub>- of allyls appear between 1140 and 1190 cm<sup>-1</sup>.<sup>[13]</sup> A weak band is detected at 1137 cm<sup>-1</sup>. Due to the shift to lower wavelength, the band may be assigned to -CH<sub>2</sub>- wagging vibrations of other alkenyls, too.

Methyl groups occur mostly in SiMex moieties that can be seen in the 3000 cm<sup>-1</sup> region, at 1407 cm<sup>-1</sup> and around 1250 cm<sup>-1</sup>. Furthermore, the strong and sharp peak at 835 cm<sup>-1</sup> indicates that generally three -CH<sub>3</sub> groups are attached to one silicon atom, while the typical signature of >SiMe<sub>2</sub> moieties at 805 cm<sup>-1</sup> is much less pronounced. When an increased incorporation of oxygen

takes place, for example at low ATMS fractions, see Figure 5, the shoulder of -(SiMe<sub>2</sub>)- increases and the peak of SiMe<sub>3</sub> decreases.

Additionally, the symmetric stretching vibration of aliphatic -CH<sub>2</sub>- appears as a shoulder at approximately 2873 cm<sup>-1</sup> and a band due to scissoring of -CH<sub>2</sub>- at 1456 cm<sup>-1</sup>. It is possible that the band at 1456 cm<sup>-1</sup> overlaps with the asymmetric bending vibration of aliphatic CH<sub>3</sub>. The symmetric bending vibration of aliphatic CH<sub>3</sub> occurs at a wavenumber of approximately 1375 cm<sup>-1</sup>. Another important structural element can be seen at 1333 cm<sup>-1</sup>, namely the C-H deformation at a tertiary carbon atom. The peaks from bending vibrations of Si-CH<sub>2</sub>-Si at 1045 cm<sup>-1</sup> and -CH<sub>2</sub>- in Si-CH<sub>2</sub>-Si at 1353 cm<sup>-1</sup> in comparison with FTIR-ATR spectra of plasma polymers made from HMDS, see Fonseca et al.<sup>[17]</sup> for example, are very small and, therefore, not visible in the Raman spectra. SiHx occurs at wavenumbers around 2110 cm<sup>-1</sup>.

The WDXS data from Section 3.3 have shown the incorporation of oxygen, which can be seen in the FTIR-ATR spectra, too. Oxygen-containing structural elements are Si-OH or C-OH absorbing between 3400 and 3200 cm<sup>-1</sup>, C=O (around 1710 cm<sup>-1</sup>), and Si-O-Si, responsible for two shoulders at lower and higher wavenumbers of the Si-CH<sub>2</sub>-Si peak. The exact positions of the corresponding peaks can be obtained by subtracting two spectra from each other which are taken from deposits with a lower and a higher oxygen concentration, respectively. The difference spectrum shows Si-O-Si peaks at approximately 1065 and 1025 cm<sup>-1</sup>. Higher amounts of oxygen appear only in an increase of Si-O-Si groups; the band areas of C=O and Si-OH or C-OH remain relatively constant.

Raman spectra of the plasma polymers show an additional peak at 606 cm<sup>-1</sup> due to the symmetric stretching vibration of Si-C. Si-Si bonds are not visible.

### 3.5 | Mass spectrometry

The relevance of ionic species for film deposition and possible ionic gas-phase polymerization processes can be visualized by ion mass spectrometry: Figure 7 shows positive ion mass spectra for two ATMS admixtures of 100 and 2000 ppm and electrode positions as indicated by the white dots in Figure 1b. These conditions have been chosen as two effects have to be distinguished when discussing mass spectrometry data from the SF-DBD. On the one hand, the plasma becomes narrower with increasing admixture and on the other hand, the influence of photo-ionization and long-lived species will increase when moving further away from the plasma

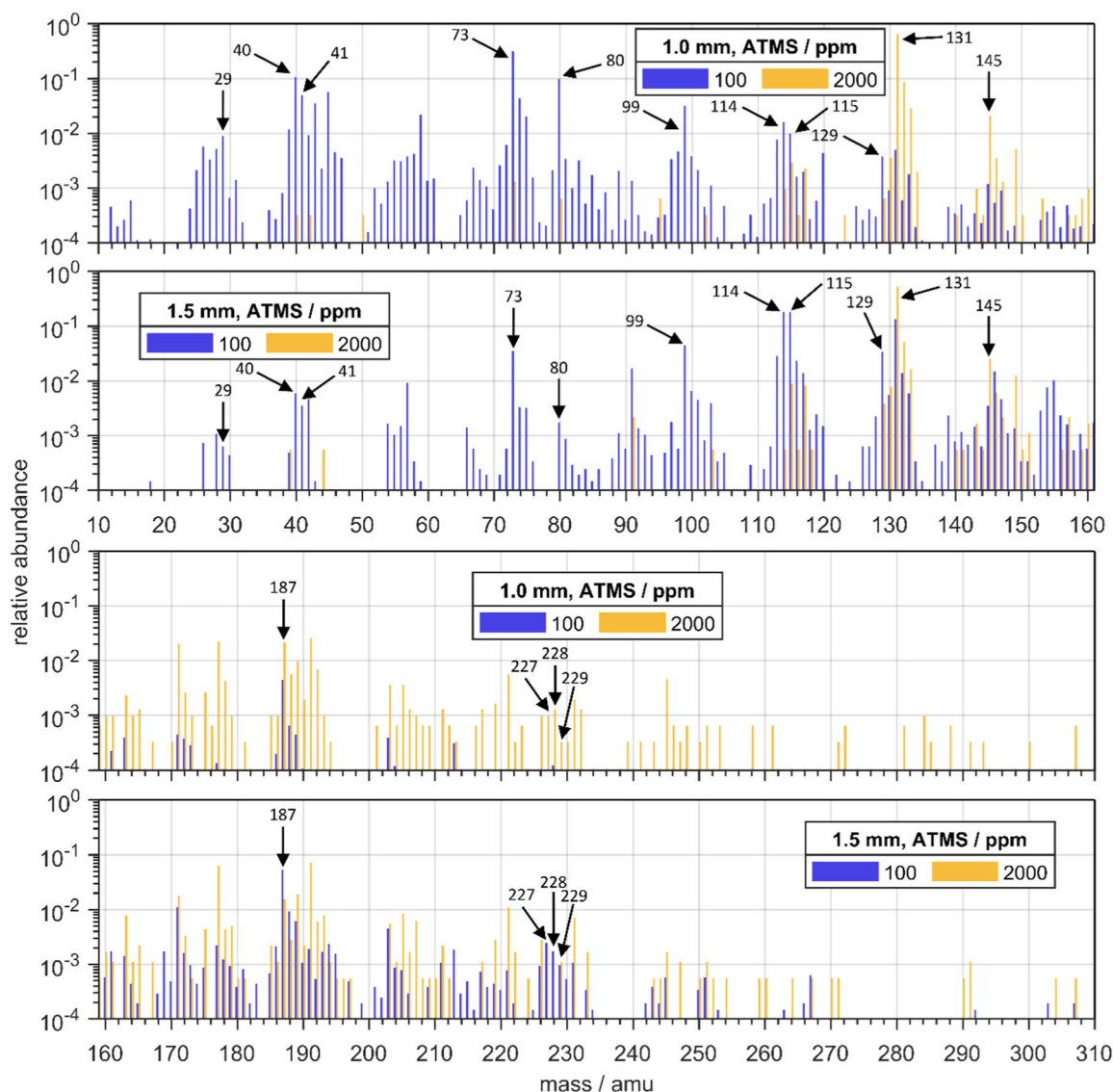


**FIGURE 7** Ion mass spectra of allyltrimethylsilane (ATMS) in a range from 10 to 310 amu at an admixture of 100 and 2000 ppm and at distances of 1.0 and 1.5 mm perpendicular to the gas flow direction.

core. To correct intensity changes in the overall ion signal, the spectra have been normalized to the total sum of all signals in the measured mass range. This allows the identification of relative changes in the ion composition when comparing different orifice positions and admixtures. The total ion signal decreases strongly with increasing distance and admixture, due to the active discharge region moving away from the orifice in both cases. This leads to an increasing uncertainty of the measured signals. The observed trends are summarized in the following.

A high amount of ATMS fragment ions is observed at masses below 114 amu, especially for the 1-mm case and low admixtures, where the orifice is closer to the discharge center and the active discharge has a larger diameter. The spectra in this mass range are dominated

by the trimethylsilyl ion at 73 amu and the ADMS ion at 99 amu, both directly related to the ATMS molecule via loss of the allyl group or a methyl group, respectively. Another directly related fragment ion is the ion at 113 amu being produced via hydrogen abstraction from the monomer. The ion at 91 amu, which is dominant below 114 amu at 1.5 mm and 2000 ppm admixture, is connected with trimethylsilyl via attachment of a water molecule. Additionally,  $C_xH_y^+$  ions are observed at low admixture and closer to the plasma core. The signals of these hydrocarbon molecules are visible in groups from 12 to 16 amu ( $CH_y^+$ ), 24 to 30 amu ( $C_2H_y^+$ ), and 36 to 44 amu ( $C_3H_y^+$ ). The signal at 45 amu could be assigned to protonated  $C_3H_8^+$ . The peaks between 50 and 60 amu are associated with species containing one silicon atom, like, for example, dimethylsilyl at 58 amu, a possible

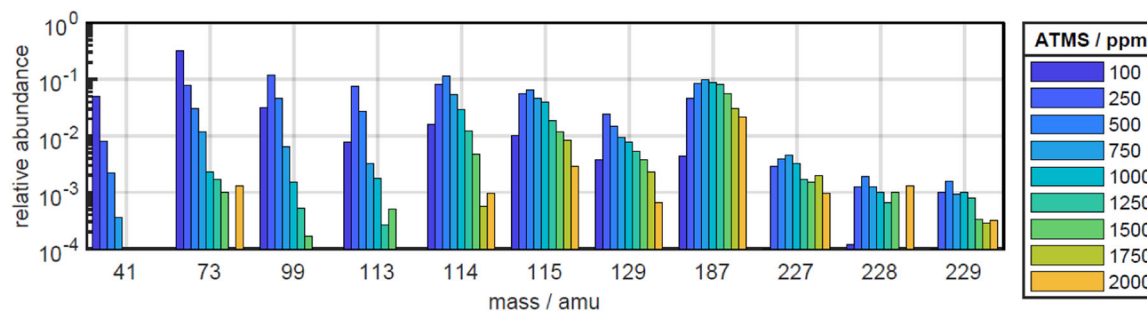


FIGURE 8 Relative ion signals normalized to the integrated ion signal as a function of allyltrimethylsilane (ATMS) admixture at selected masses related to the  $\text{ATMS}^{++}$  cation. Data measured at a distance of 1.0 mm.

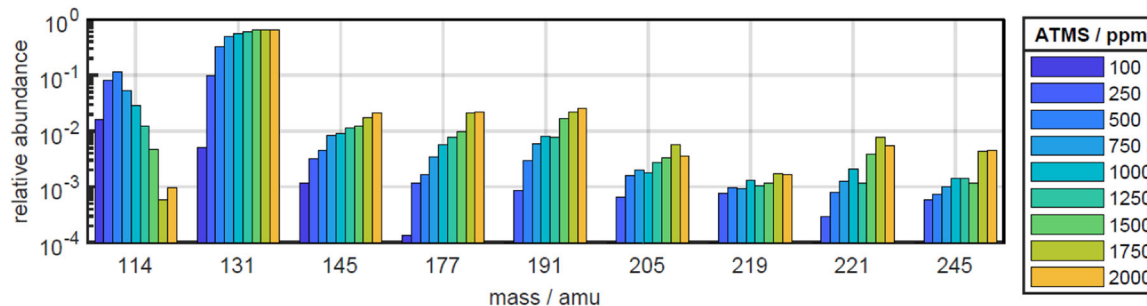


FIGURE 9 Relative ion signals normalized to the integrated ion signal as a function of allyltrimethylsilane (ATMS) admixture at selected masses larger than the mass of the  $\text{ATMS}^{++}$  cation (also shown for reference). Data measured at a distance of 1.0 mm.

fragment of  $\text{Me}_3\text{Si}^+$ .<sup>[18]</sup>  $\text{Ar}^+$  at mass 40 and  $\text{Ar}^{2+}$  at mass 80 are observed as well. Fragment ions disappear quickly with increasing ATMS admixture, see, for example, the 41, 73, and 99 amu ions in Figure 8, and the monomer ion and the ion at mass 131 become dominant: Based on the measured isotope signals at 132 and 133 amu, only a very small fraction of the signal at 131 amu can be attributed to the pentamethyldisilyl cation [ $\text{PMDS}^+$ ,  $(\text{CH}_3)_3\text{SiSi}(\text{CH}_3)_2^+$ ], a possible fragment of  $\text{HMDS}^{++}$ , see Dávalos and Baer<sup>[19]</sup> for example. The main part of the signal can either be attributed to an incorporation of an OH moiety into the ATMS molecule or an attachment of water to the 113 amu fragment. For future experiments, attempts should be made to decrease the overall water concentration in the plasma zone.

The ion at mass 131 seems to get stabilized and is less reactive when compared to  $\text{ATMS}^{++}$  ions. This is corroborated by the fact that the absolute ion signal at mass 131 is only varying slightly with the admixture and is probably proportional to the water impurity level in the feed gas mixture.

Ions with masses above 114 amu are increasingly observed at larger distances from the plasma symmetry axis probably due to a longer residence time of the ions in the gas phase before sampling. Fragments of  $\text{ATMS}^{++}$  ions below the mass of 73 amu are almost absent in the

measurement at 1.5 mm distance. Possible reasons of this effect, for example, ablation processes that can occur as a result of filaments which are repeatedly ignited on the edge of the orifice for small distances between the orifice and high-voltage electrode, were mentioned earlier.

The formation of ions with masses of 115, 129, and 187 amu becomes possible via addition or transfer reactions of  $\text{H}^+$ , a methyl cation, or a trimethylsilyl cation with the monomer, respectively. Especially the abundance of the ion with 115 and 187 amu is quite high, see Section 4.2.1 for more information. Interestingly, an increase in the monomer fraction results at first in a rise in these signals, for example, for the 187 amu species up to 750 ppm, and afterward a decline can be observed, similar to the  $\text{ATMS}^{++}$  monomer ion, see Figure 8.

Ions with masses 227, 228, and 229 amu indicate reactions of the fragment ion at 113 amu,  $\text{ATMS}^{++}$ , or protonated  $\text{ATMS}^{++}$  with another ATMS molecule. The fact that these signals are increasing up to monomer fractions of 250 or 500 ppm and decreasing with further increase of the ATMS admixture could be an indicator that these ions can polymerize further to larger masses. However, the mass 227 can also be correlated to the 187 amu ion with an attached argon atom since the signals are rather low.

Figure 9 shows the relative signals of selected ions with masses higher than the monomer mass at 145, 177,

191, 205, 219, 221, and 245 amu<sup>1</sup> as a function of the precursor admixture. The relative signals are continuously increasing with increasing ATMS admixture. Mass 145 amu can be assigned to a product ion as a result of a reaction of Me<sub>3</sub>Si<sup>+</sup> and neutral dimethylsilylene (Me<sub>2</sub>-Si=CH<sub>2</sub>, 72 amu) or TMS (Me<sub>4</sub>Si, 88 amu). Both can possibly be formed in the plasma. In the latter reaction mechanism, methane is abstracted, see Klevan and Munson.<sup>[22]</sup>

Measurements on the plasma axis were not possible due to fast deposition rates and large ion signals, but the data measured at 1.0 and 1.5 mm provide clear hints that ATMS<sup>++</sup> cations are generated in the plasma and that the average ion mass is growing with increasing ATMS admixture. However, it is questionable whether measurements near the center of the deposit reflect the actual plasma processes, see the discussion above. Therefore, improvements of the plasma ignition on the sampling orifice are necessary to avoid ablation processes and high ion signals in general.

Table 4 shows the main species from the mass spectrum with the corresponding ion masses in amu, the chemical composition, and how the detected mass corresponds to the molar mass of the other detected species. Some masses are formed due to clustering of ATMS-related cations either with H<sub>2</sub>O molecules or with argon ions. These clusters can be formed either in the gas phase or in the adiabatic gas expansion in the sampling orifice before its transition to molecular flow.

Unfortunately, the method is not able to work with good sensitivity beyond *m/z* of about 300. The lack of detection of ions with *m/z* 301 which would prove the second step of a polymerization via the path Me<sub>3</sub>Si<sup>+</sup> + *n* × M, however, is taken as an indication that this mechanism does not take place in the gas phase.

## 4 | DISCUSSION

The nearly circular symmetry of deposits obtained in the above-described experiments suggests that the transport of growth species from the discharge volume to the substrate takes place in a time which is much shorter than the gas residence time of typically 2 ms. As it will become apparent later, “growth species” has to be understood in a more general sense, including

catalytically active chemical species able to transform the precursor into a film and polymerization initiators, in addition to the deposited material itself. Using the expression  $t_D = h^2/\pi/D$  to calculate the diffusion time with typical values  $D = 0.05 \text{ cm}^2/\text{s}$  and  $h = 0.1 \text{ cm}$ , resulting in  $t_D = 64 \text{ ms}$ , it becomes evident that diffusive mass transport is too slow to explain the characteristic shape of the deposits. The lack of any deposition beyond the area directly in contact with the discharge excludes also that photochemical processes due to vacuum ultraviolet irradiation from the discharge play a dominating role. Therefore, one is left with the drift of positive ions in the electric fields of a temporarily established cathode fall, resulting in transport times in the order of a few  $\mu\text{s}$ . The open question and main subject of the following discussion is the mechanism by which the deposit can grow by up to 540 amu while one elementary charge is transferred to the substrate.

Results of electrical characterization as well as an overall diffuse plasma appearance support the relevance of Penning processes: Extinction voltages (Figure 2) strongly decline up to ATMS fractions between 250 and 300 ppm. This is similar to experiments reported by Heylen, where decreasing sparking voltages were observed for various hydrocarbons, when the fraction of the hydrocarbon was increased from 3 to 300 ppm.<sup>[23–25]</sup> For monomer fractions beyond 300 ppm, the plasma appears less diffuse and an increase of the extinction voltage from the minimum of 1 up to 1.4 kV for 2000 ppm can be seen, similar to results for HMDSO in argon, see Figure 2. Similar effects have already been reported and discussed in Yamane<sup>[26]</sup> and will not be discussed further here.

It should be noted that dissociation into neutrals is expected to take place after energy transfer from Ar\* to ATMS in addition to (dissociative) ionization, probably with larger frequency than Penning ionization.<sup>[27]</sup>

### 4.1 | Wet-chemistry of ATMS

Before entering into a discussion of the present experimental results, a short account of relevant wet-chemical reactions of ATMS seems appropriate to draw conclusions regarding the relevant deposition mechanisms discussed in Sections 4.2 and 4.3. In general, radical polymerization of allyl monomers leads to polymers with comparatively low molecular weight. The reason for this behavior is degradative chain transfer, where the active center is transferred from the growing chain to the monomer, leading to its termination.<sup>[28]</sup> For ATMS, Mikulášov determined degrees of polymerization  $DP_n$  ranging from 3.8 to 4.7 and an activation energy of

<sup>1</sup>Ions with masses of 191, 205, 207, and 221 amu are produced by cationic polymerization reactions in HMDSO plasmas, Alexander et al.<sup>[20]</sup> and Jiao et al.<sup>[21]</sup> Due to water and oxygen impurities, it is reasonable to assume that such ions can be formed here, too, but the isotope signals are not in accordance with the chemical structures of these ions.

TABLE 4 Detected ions: mass, linear formula, chemical composition, and possible reaction pathways.

Mass (amu)	Linear formula	Chemical composition	Connection to other masses
40	Ar <sup>+</sup>	Ar	40
41	ArH <sup>+</sup> , CH <sub>2</sub> CH=CH <sub>2</sub> <sup>+</sup>	ArH, C <sub>3</sub> H <sub>5</sub>	40 + 1, M - 73
58	(CH <sub>3</sub> ) <sub>2</sub> Si <sup>+</sup>	C <sub>2</sub> H <sub>6</sub> Si	73-15
73	(CH <sub>3</sub> ) <sub>3</sub> Si <sup>+</sup>	C <sub>3</sub> H <sub>9</sub> Si	M-41
91	(CH <sub>3</sub> ) <sub>3</sub> Si <sup>+</sup> + H <sub>2</sub> O, (CH <sub>3</sub> ) <sub>3</sub> SiOH <sub>2</sub> <sup>+</sup>	C <sub>3</sub> H <sub>11</sub> SiO	73 + 18
99	(CH <sub>3</sub> ) <sub>2</sub> Si <sup>+</sup> CH <sub>2</sub> CH=CH <sub>2</sub>	C <sub>5</sub> H <sub>11</sub> Si	M-15
113	(CH <sub>3</sub> ) <sub>3</sub> SiCHCH=CH <sub>2</sub> <sup>+</sup> , (CH <sub>3</sub> ) <sub>3</sub> Si <sup>+</sup> + Ar	C <sub>6</sub> H <sub>13</sub> Si, C <sub>3</sub> H <sub>9</sub> SiAr	M - 1, 73 + 40
114	(CH <sub>3</sub> ) <sub>3</sub> SiCH <sub>2</sub> CH=CH <sub>2</sub> <sup>+</sup>	C <sub>6</sub> H <sub>14</sub> Si	M
115	(CH <sub>3</sub> ) <sub>3</sub> SiCH <sub>2</sub> CH <sup>+</sup> CH <sub>3</sub>	C <sub>6</sub> H <sub>15</sub> Si	M + 1
129	(CH <sub>3</sub> ) <sub>3</sub> SiCH <sub>2</sub> CH <sup>+</sup> CH <sub>2</sub> CH <sub>3</sub> <sup>+</sup>	C <sub>7</sub> H <sub>17</sub> Si	M + 15
131	(CH <sub>3</sub> ) <sub>3</sub> SiCH <sub>2</sub> CH <sup>+</sup> CH <sub>2</sub> OH, (CH <sub>3</sub> ) <sub>3</sub> SiCHCH=CH <sub>2</sub> <sup>+</sup> + H <sub>2</sub> O	C <sub>6</sub> H <sub>15</sub> SiO	M + 17, 113 + 18
145	(CH <sub>3</sub> ) <sub>3</sub> Si-CH <sub>2</sub> -Si <sup>+</sup> (CH <sub>3</sub> ) <sub>2</sub>	C <sub>6</sub> H <sub>17</sub> Si <sub>2</sub>	73 + 72
146	(CH <sub>3</sub> ) <sub>3</sub> SiSi(CH <sub>3</sub> ) <sub>3</sub> <sup>+</sup>	C <sub>6</sub> H <sub>18</sub> Si <sub>2</sub>	73 + 73
149	(CH <sub>3</sub> ) <sub>3</sub> SiCH <sub>2</sub> CH <sup>+</sup> CH <sub>2</sub> OH + H <sub>2</sub> O, (CH <sub>3</sub> ) <sub>3</sub> SiCHCH=CH <sub>2</sub> <sup>+</sup> + 2 H <sub>2</sub> O	C <sub>6</sub> H <sub>17</sub> SiO <sub>2</sub>	131 + 18
153	(CH <sub>3</sub> ) <sub>3</sub> SiCHCH=CH <sub>2</sub> <sup>+</sup> + Ar	C <sub>6</sub> H <sub>13</sub> SiAr	113 + 40
154	(CH <sub>3</sub> ) <sub>3</sub> SiCH <sub>2</sub> CH=CH <sub>2</sub> <sup>+</sup> + Ar	C <sub>6</sub> H <sub>14</sub> SiAr	M + 40
155	(CH <sub>3</sub> ) <sub>3</sub> SiCH <sub>2</sub> CH <sup>+</sup> CH <sub>3</sub> + Ar	C <sub>6</sub> H <sub>15</sub> SiAr	115 + 40
163	(CH <sub>3</sub> ) <sub>3</sub> Si-CH <sub>2</sub> -Si(CH <sub>3</sub> ) <sub>2</sub> <sup>+</sup> + H <sub>2</sub> O	C <sub>7</sub> H <sub>19</sub> SiO <sub>2</sub>	145 + 18
171	(CH <sub>3</sub> ) <sub>3</sub> SiCH <sub>2</sub> CH <sup>+</sup> CH <sub>2</sub> OH + Ar, (CH <sub>3</sub> ) <sub>3</sub> SiCHCH=CH <sub>2</sub> <sup>+</sup> + H <sub>2</sub> O + Ar	C <sub>6</sub> H <sub>14</sub> SiOAr	131 + 40
187	(CH <sub>3</sub> ) <sub>3</sub> SiCH <sub>2</sub> CH <sup>+</sup> CH <sub>2</sub> Si(CH <sub>3</sub> ) <sub>3</sub> <sup>+</sup>	C <sub>9</sub> H <sub>23</sub> Si <sub>2</sub>	M + 73
227	(CH <sub>3</sub> ) <sub>3</sub> SiCH[CH <sub>2</sub> CHCH <sub>2</sub> Si(CH <sub>3</sub> ) <sub>3</sub> ]CHCH <sub>2</sub> <sup>+</sup> , (CH <sub>3</sub> ) <sub>3</sub> SiCH <sub>2</sub> CH <sup>+</sup> CH <sub>2</sub> Si(CH <sub>3</sub> ) <sub>3</sub> + Ar	C <sub>12</sub> H <sub>27</sub> Si <sub>2</sub> , C <sub>9</sub> H <sub>23</sub> Si <sub>2</sub> Ar	M + 113, 187 + 40
228	(CH <sub>3</sub> ) <sub>3</sub> SiCH <sub>2</sub> CH[CH <sub>2</sub> CHCH <sub>2</sub> Si(CH <sub>3</sub> ) <sub>3</sub> ]CH <sub>2</sub> <sup>+</sup>	C <sub>12</sub> H <sub>28</sub> Si <sub>2</sub>	M + M
229	(CH <sub>3</sub> ) <sub>3</sub> SiCH <sub>2</sub> CH[CH <sub>2</sub> CHCH <sub>2</sub> Si(CH <sub>3</sub> ) <sub>3</sub> ]CH <sub>3</sub> <sup>+</sup>	C <sub>12</sub> H <sub>29</sub> Si <sub>2</sub>	M + 115

144 kJ/mol,<sup>[29]</sup> far beyond the range of activation energies for the addition of phenyl or alkyl radicals to unsaturated compounds, 18–44 kJ/mol.<sup>[30]</sup> High-molecular weight, partially crystalline, isotactic polymers are accessible from ATMS or other allyltrialkylsilanes by Ziegler–Natta polymerization using a TiCl<sub>4</sub>/AlR<sub>3</sub> Ziegler catalyst (*R* = ethyl or isobutyl).<sup>[12,31,32]</sup> Control of tacticity is possible by the use of suitable metallocene catalysts.<sup>[33,34]</sup> By addition of carbenium ions R<sup>+</sup> to the terminal C atom, allylsilanes, CH<sub>2</sub>=CH-CH<sub>2</sub>-SiR'<sub>3</sub>, generally form beta-silicon-stabilized carbenium ions which subsequently react with the counter ion of R<sup>+</sup> under loss of R'<sub>3</sub>Si<sup>+</sup>, resulting in R-CH<sub>2</sub>-CH=CH<sub>2</sub>.<sup>[35]</sup> Therefore, ATMS is often used as a “capping agent” to

terminate living cationic polymerization processes, giving an allyl-terminated chain end.<sup>[36]</sup> An oligomerization of ATMS can only be achieved under certain conditions by Lewis or Brønsted acids.<sup>[37]</sup> The AlCl<sub>3</sub>-initiated polymerization of neat ATMS, described as “vigorous,” results in an oily, distillable material with an 18% (relative) silicon deficit in the elemental analysis.<sup>[38]</sup>

## 4.2 | Gas-phase processes

The main objective of the following discussion is to give a reasonable explanation of the large average mass up to 540 amu, deposited per transferred elementary

charge (Figure 4). Because of the absence of strongly electronegative elements such as oxygen, fluorine, or chlorine, contributions of negative ions to the film deposition are neglected. In the following, the possibility of free-radical or cationic gas-phase polymerization will be considered first.

#### 4.2.1 | Role of cationic gas-phase polymerization of ATMS

In classical polymer chemistry, initiation of cationic polymerization of alkenyl monomers by stable carbenium salts as well as by “bare” carbenium ions without anions, prepared by radiolysis, photochemical ionization, or other physico-chemical means, is well known.<sup>[39]</sup> However, in the paper by Stillwell et al., no further addition reactions of the adduct ions with 187 amu ( $[\text{ATMS}+\text{SiMe}_3]^+$ ), 213 amu ( $[\text{ATMS}+\text{ADMS}]^+$ ), or 229 amu ( $[\text{ATMS}+\text{H}+\text{ATMS}]^+$ ) to the parent compound ATMS were reported.<sup>[7]</sup> An inspection of the mass-spectral information reported above shows that under the present experimental conditions, too, no ions with  $m/z$  beyond 229 are observed, which could be interpreted in terms of repeated addition of ATMS in a cationic polymerization process, eventually resulting in ions with  $m/z$  beyond 500.

Another argument against a cationic gas-phase mechanism for ATMS polymerization can be based on the short duration of individual microdischarges with cathodic substrate. At  $x_M = 2000$  ppm ( $n_M = 4.9 \times 10^{16} \text{ cm}^{-3}$ ), the discharge current has a full width at half maximum of about  $0.2 \mu\text{s}$ . In order to consecutively add four ATMS molecules to the initiating carbenium ions or the chain end, only  $0.05 \mu\text{s}$  is available on average for each step. The average rate coefficient for these steps would have to be at least  $4.1 \times 10^{-10} \text{ cm}^3 \text{ s}^{-1}$ . This is about 40% of the ion-molecule capture rate coefficient ( $k_{\text{ADO}} = 1.0 \times 10^{-9} \text{ cm}^3 \text{ s}^{-1}$ <sup>[40]</sup>), calculated with a polarizability volume of  $14.5 \text{ \AA}^3$ <sup>[41]</sup> and a dipole moment of  $0.58 \text{ D}$ <sup>[42]</sup> for ATMS, and assuming a molecular weight of 250 amu for the oligomeric ion. However, it has been observed for a range of gas-phase polymerizations involving carbenium ions that only the first step occurs with a rate near the capture rate, while subsequently the rate coefficient drops by orders of magnitude.<sup>[43–45]</sup> Therefore, the discharge duration is not sufficient to allow the formation of oligomers with four monomer units via a cationic propagation process starting with the microdischarge.

#### 4.2.2 | Role of free-radical gas-phase polymerization of ATMS

A similar argument can be put forward against film formation by a radical polymerization process in the discharge volume, followed by a charge transfer reaction to form an oligomeric cation: In this case, the chain growth would have to take four steps within the residence time of about 2 ms. This would require a propagation rate coefficient  $k_p$  of at least  $4 \times 10^{-14} \text{ cm}^3 \text{ s}^{-1}$ , at least four orders of magnitude beyond the values for polymerization of, for example, acrylonitrile, vinyl chloride,<sup>[46]</sup> or styrene.<sup>[47]</sup> In view of the large activation energy reported for free-radical polymerization of ATMS, 144 kJ/mol,  $k_p$  for this process should be even smaller. The lack of a significant influence of the average gas flow velocity (Table 2), too, provides strong evidence that the deposition process does not directly involve neutral products of plasma-chemical processes in the discharge.

### 4.3 | Surface processes

#### 4.3.1 | Evidence of cationic surface polymerization of ATMS

After what has been stated above, film formation by deposition of ions with average masses up to 540 amu, formed in the discharge volume, seems very unlikely. A strong argument in favor of a surface process can be derived from the experiments with varied frequency, see Table 2: The increase of deposited mass per Faraday of transferred charge with decreasing excitation frequency can be explained by surface polymerization of ATMS molecules initiated by the radical ion  $\text{ATMS}^{\bullet+}$  or by any of the ions formed in ion-molecule reactions, such as  $\text{Me}_3\text{Si}^+$  or its addition product with ATMS, with  $m/z$  187. During the microdischarge with negative polarity, these ions are drifting to the substrate on negative potential, acquiring a mean kinetic energy in the order of 1 eV, as calculated with equation 2.31 in Raizer.<sup>[48]</sup> It appears reasonable to assume that on average 50% of these ions lose their positive charge by recombination with electrons left in shallow traps on the growing pp-ATMS film from the previous microdischarge in the positive half-wave. The rest will stick to the surface with preserved charge as “soft-landed” ions<sup>[49,50]</sup> until all positive ions on the surface recombine with electrons in the next microdischarge with opposite polarity. The lifetime of the positive surface charge therefore equals half of the excitation voltage period,  $T/2$ .

Owing to electrostatic image forces,<sup>[51]</sup> the surface-binding energy of these ions, considered as point charges with an estimated distance  $d = 0.2$  nm from a dielectric half space with a dielectric constant of  $\epsilon = 2.3$  (value for a polycarbosilane<sup>[52]</sup>), is in the order of 1 eV. These ions are therefore considered as chemisorbed.

The experimental data can now be explained by the following hypotheses: During the time  $T/2$ , the ions  $I^+$  are able to react either by (i) initiating a cationic polymerization process, resulting in a growing chain  $IM_n^{+2}$ , or by (ii) deactivation as a catalyst by reaction with a neutral Lewis base B, such as physisorbed water molecules or chemisorbed oxygen in the form of Si–O–Si or Si–O–C moieties at the film surface. The latter reaction will also terminate the growing chain  $IM_n^+$ . Eventually, all chains are terminated at  $t = T/2$  by recombination with electrons transferred to the surface during the following microdischarge with positive polarity.

A simple equation for the dependence of the deposited mass per Faraday of transferred charge can be derived using the assumption that all addition reactions with M,  $IM_n^+ + M \rightarrow IM_{n+1}^+$  ( $n \geq 0$ ) have the same rate coefficient  $k_M$  ( $\text{cm}^2 \text{mol}^{-1} \text{s}^{-1}$ ) and all reactions with the Lewis base B,  $IM_n^+ + B \rightarrow IM_n^+B$ , where  $IM_n^+B$  is unreactive toward M, have the same rate coefficient  $k_B$  ( $\text{cm}^2 \text{mol}^{-1} \text{s}^{-1}$ ).

Then, the equation for the growth rate of the film mass  $m_F$  can be written as a rate equation for bimolecular surface reactions between adsorbed monomer molecules M and cationic chains  $IM_n^+$ :

$$\frac{d}{dt} m_F(t) = M_M S k_M \Gamma_M \Gamma_{C^+}(t) = M_M S k_M \Gamma_M \Gamma_{C^+}(0) \exp(-k_B \Gamma_B t)$$

$$\Gamma_{C^+}(t) \equiv \sum_{n=0}^i \Gamma_{IM_n^+}(t), \quad (1)$$

where  $M_M$  is the molecular mass of the monomer,  $S$  the surface area, and  $\Gamma_i$  the surface coverage of species  $i$  (mole per unit area).  $\Gamma_{C^+}$  represents the sum of  $\Gamma$ 's of all active species  $IM_n^+$  and is decaying exponentially in time due to the reaction with B. It is assumed that the surface coverages of species M and B are kept constant in time by a rapid exchange with the gas-phase (equilibrium adsorption) and/or virtually constant surface coverage by chemisorbed oxygen.

The mass growth within the half period following a microdischarge with negative polarity (i.e., cathodic

substrate) is obtained by integration of Equation (1). Here, it is assumed that the deposition of ions takes virtually no time, that is, the generation of  $I^+$  centers is already complete at the start of the half-period at  $t = 0$ . The result is

$$m_F(T/2) = m_I + \frac{M_M S k_M \Gamma_M \Gamma_{C^+}(0)}{k_B \Gamma_B} \times [1 - \exp(-k_B \Gamma_B T/2)], \quad (2)$$

where  $m_I$  is the mass of the ions deposited at  $t = 0$ . It is assumed that half of the ions arriving at  $t = 0$  are neutralized instantly by trapped electrons and the other half is neutralized at  $t = T/2$ . It is assumed further that the full mass of the initiating ions contributes to film growth. Then, with  $m_I = 2\Gamma_{C^+}(0)SM_I$  and  $\Gamma_{C^+}(0)S = q_i/(2N_A e)$  ( $F$  = Faraday constant), the result for  $m_q = m_F F/q_i$  can be written as:

$$m_q(T/2) = M_I + M_M \frac{1}{2} \frac{k_M \Gamma_M}{k_B \Gamma_B} \times \left[ 1 - \exp\left(-k_B \Gamma_B \frac{T}{2}\right) \right]. \quad (3)$$

In the limits of high and low frequencies, this equation approaches

$$m_q(T/2)_{\text{highf}} = M_I + M_M \frac{k_M \Gamma_M T}{2}, \quad (4)$$

and

$$m_{q,\text{lowf}} = M_I + M_M \frac{1}{2} \frac{k_M \Gamma_M}{k_B \Gamma_B}, \quad (5)$$

respectively.

The functional dependence on  $T/2$  is reasonably well in line with the experimental data, see Figure 10, where fits were made of a nonlinear function

$$m_q(T/2) = M_I + A \times \left[ 1 - \exp\left(-B \frac{T}{2}\right) \right], \quad (6)$$

with different choices for the constant  $M_I$ . In the figure legend, the fit parameter  $A$  is written as a product with a factor  $M_M = 114$ , led by the hypothesis that the polymerization propagates by addition of ATMS molecules. Although the choice of  $M_I = 73$  g/mol ( $\text{Me}_3\text{Si}^+$ ) seems to give a better agreement with experimental data, see the comparatively large error bars,  $M_I = 187$  g/mol ( $\text{Me}_3\text{Si}-\text{CH}_2-\text{CH}^+-\text{CH}_2-\text{SiMe}_3$ ) is in better agreement with Figure 4 ( $m_q$  vs.  $x_M$ ), in which a linear fit yields an intercept of 210. The mass spectrometry data further

<sup>2</sup>“ $IM_n^+$ ” represents a chain I-M-M...M-M<sup>+</sup> consisting of an initiator I and  $n$  monomer units M, added via the double bond and carrying a positive charge at a triply bonded carbon atom.

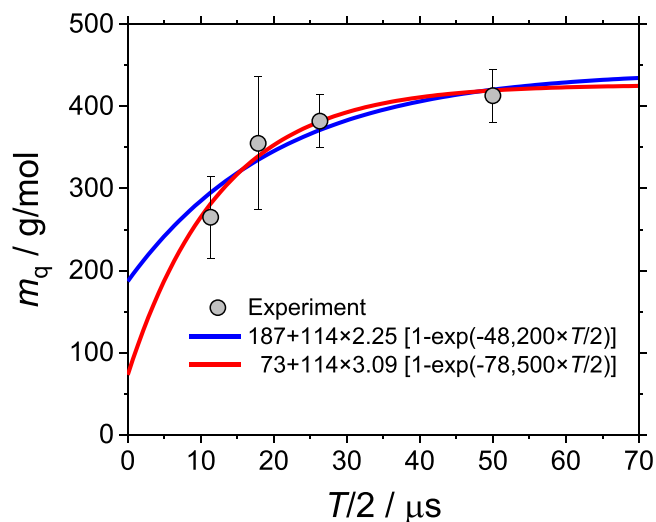


**FIGURE 10** Effect of frequency variation; experimental data plotted as a function of  $T/2$  and nonlinear fits obtained with the assumption that the initiating ion  $I^+$  has the mass 73 amu (red) and 187 amu (blue).

support this observation, as the  $\text{Me}_3\text{Si}^+$  signal is orders of magnitude smaller than the 187 amu signal, see Figure 8.

It should be noted that the decrease of  $m_q$  with growing frequency is not due to monomer depletion by the increased consumption: In the case of depletion,  $m_q$  should increase with growing gas flow rate, which is not observed, see the last two entries in Table 2.

A similar cationic chain growth mechanism as proposed above was already postulated by Thompson and Mayhan for low-pressure radiofrequency (RF)-plasma polymerization of styrene.<sup>[53]</sup> An example of cationic surface polymerization from the vapor phase without plasma assistance can be found, for example, in Bose et al.,<sup>[54]</sup> where the  $\text{BF}_3$ -initiated ring-opening polymerization of ethylene oxide to prepare antifouling poly(ethylene oxide) films is described. Another example is a paper by Gao et al. in which the cationic polymerization of styrene initiated by  $\text{TiCl}_4$  in the presence of water is reported. That process enables a deposition rate two orders of magnitude larger than free-radical initiated chemical vapor deposition (iCVD).<sup>[55]</sup>

The present experiments with varied substrate temperature performed at  $f = 19$  kHz ( $T/2 = 26.3$  μs) and  $x_M = 1000$  ppm reveal a surprisingly small temperature dependence of  $m_q$ . An Arrhenius plot results formally in an “activation energy”  $E_A$  of  $-2.1$  kJ/mol. Close to the low-frequency limit, the  $T$  dependence of  $m_q$  is mainly determined by the  $T$  dependence of the fraction in Equation (5).  $E_A$  is the difference of heats of adsorption of M and B plus the difference in activation energies for the propagation reaction with M and the reaction with

base B. The lack of corresponding data precludes a further discussion of  $E_A$ .

### 4.3.2 | Role of radical surface polymerization of ATMS

Several thin film deposition processes have already been described in the literature which more or less resemble the polymerization initiated at the gas–solid interface by species originating from the plasma, as outlined above. The iCVD method developed in the group of Karen Gleason has been already known for several years.<sup>[56]</sup> Here, the surface processes are mostly free-radical polymerizations, where an initiating species is generated by thermal dissociation on a hot filament or by photo- and low-pressure plasma-chemical means. A kinetic model of iCVD from alkyl acrylates was published by Lau and Gleason.<sup>[57]</sup>

In the past, pulsing of the discharge has often been applied to reveal the effect of long-lived surface radicals on the plasma-polymerization process: Raising the pause length can increase the film thickness per cycle, see, for example, Klages et al.<sup>[58]</sup> for the deposition of glycidyl methacrylate, where the reaction of intact monomer molecules with surface radicals generated during the pulses plays a prominent role. As the deposition of neutral reaction products from the gas phase is avoided by the SF-DBD setup, experiments with 60-μs pulses and pauses of 240 or 480 μs length can reveal whether surface grafting processes, where the ATMS monomer reacts with a surface free radical, are of relevance: Table 2 shows no clear trend of  $m_q$  for increased pause times, which suggests that radical surface polymerization is not significant.

## 4.4 | The molecular structure of films deposited from ATMS

Thin films deposited from ATMS are most probably highly cross-linked, as evidenced by solvent-exposure experiments, see Section 3.4.

FTIR-ATR measurements show all bands (Table 4) which are expected for a material with the composition I-Mn-T with a terminal residue T, as to be expected based on the proposed cationic chain growth mechanism. An obvious example of T is an OH group from chain termination by water,  $\text{B} = \text{H}_2\text{O}$ .

However, there are also several IR bands that cannot be explained by the idealized chain structure I-Mn-T, namely Si–H, Si–CH<sub>2</sub>–Si, and –SiMe<sub>2</sub>– bands, when oxygen-containing moieties are not considered. In

addition to the obvious cross-linking, these bands may result from rearrangements within cations or chain transfer and chain branching. Cross-linking is, to a lesser or greater extent, accompanying plasma polymerization.<sup>[59,60]</sup> Formation of chain cross-links and chain branches during plasma-initiated cationic polymerization of styrene was already discussed in some detail in Thompson and Mayhan.<sup>[53]</sup> For specific mechanisms in plasma polymerization of organosilanes, see papers by Wrobel et al.<sup>[61]</sup> and papers cited therein.

Branching of chains is expected, for example, when an incoming ion  $I^+$  is not chemisorbed but reacts with the deposit under methide or hydride transfer and formation of a cationic surface site to which subsequent addition of ATMS molecules takes place.<sup>[62]</sup>

Last but not the least, skeletal rearrangements are potential reasons for the appearance of IR vibrational bands which cannot be explained in terms of the ideal polymer structure I-Mn-T. Organic chemistry knows a large number of rearrangements in carbocations by 1,2-sigmatropic shift of a substituent (H, alkyl, or aryl) from a neighboring carbon atom to the triply bonded, charged C atom.<sup>[63]</sup> In poly(4-methyl-1-pentene) obtained with Lewis acid catalysts, for example, five different repeating units were identified, resulting from shifts of H or  $CH_3$  in carbocations.<sup>[64]</sup> For related rearrangements in organosilanes chemistry, see the article by Albers et al. and publications cited therein.<sup>[65]</sup>

WDXS measurements, see Figure 5, show a carbon-to-silicon ratio decreasing from 6.0, obtained with 50 ppm ATMS, to 5.0 for 100 ppm ATMS. For larger  $x_M$ , the ratio declines more gradually to 4.7 for 2000 ppm. Two different aspects are of relevance, when referring to these data: (i) As Figure 8 shows, the chemical composition of the initiating ion  $I^+$  can change with the monomer fraction, as transfer reactions from  $ATMS^{*+}$  ( $[C]/[Si] = 6$ ) to ATMS to form the 187 amu ion ( $[C]/[Si] = 4.5$ ) become more probable. Subsequent addition of ATMS ( $[C]/[Si] = 6$ ) should cause an increase of the  $[C]/[Si]$  ratio for larger monomer fractions. This was, however, not observed; about 1C atom per Si is lacking. One possible reason for the lack of carbon is a loss of methyl groups as a consequence of UV irradiation or of the electron-ion recombination process.

An interesting aspect of FTIR-ATR and WDXS measurements on the pp-ATMS is the strong similarity to thin films produced at low pressure (100 Pa) with RF excitation. FTIR spectra from samples produced in the present investigation closely coincide with a spectrum reported by Talib et al.,<sup>[66]</sup> suggesting that plasma-chemical processes are basically similar. Investigations by Westwood as well as Alexander et al. suggest that under specific low-pressure conditions, the

polymerization process is of cationic nature.<sup>[20,67]</sup> In the case of positive bias voltages, no thin film deposition of vinyl chloride was observed, indicating that the plasma polymerization process is driven by cations.<sup>[67]</sup> Additionally, Alexander concludes that the deposition of HMDSO at low pressure and especially low power is due to the transport of cations and products of polymerization in the gas phase to the surface.<sup>[20]</sup> Interestingly, Talib et al. state that only radicals are forming the thin film<sup>[66]</sup> in contrast to the ionic deposition and polymerization mechanism proposed in the present paper.

## 5 | CONCLUSIONS

Plasma-enhanced thin film deposition with SF-DBDs in mixtures of argon and ATMS (MW = 114.26 g/mol) was investigated to unravel the underlying deposition mechanism(s). The main focus of the studies was to explain the high average film masses deposited per Faraday of transferred charge  $m_q$ , up to 540 g/mol for an ATMS fraction of 2000 ppm.

Results of film deposition experiments combined with electrical and mass spectrometric discharge characterization led to the conclusion that the predominant film deposition mechanism is a cationic surface polymerization process. The SF-DBD discharge, characterized by the typical signatures of Penning ionization such as a low ignition voltage and an overall diffuse optical appearance, acts as a source of ions. Predominant are the molecular ion,  $ATMS^{*+}$ , the trimethylsilyl cation  $Me_3Si^+$ , as well as the adduct of  $Me_3Si^+$  and ATMS. A deposition sequence is started with the deposition of cations  $I^+$  during a microdischarge with negative polarity. During the following half period, monomer molecules M are added to  $I^+$  and to the growing cationic polymer. An individual chain process is terminated by the adsorption of a Lewis base B or by the uptake of an electron during the following microdischarge event with positive polarity.

From mass spectrometry data, there is no evidence that cationic gas-phase addition processes with more than one ATMS molecule play an important role. Major contributions by deposition of large cations with  $m/z$  beyond 187 can therefore be excluded. The deposition of neutral gas-phase polymerization products can also be ruled out because a variation of gas residence times has virtually no influence on  $m_q$ . Incorporation of ATMS due to reactions with surface free radicals is excluded because experiments with varied pulse/pause ratio did not result in the expected significant increase in the deposition rate with pause durations.

## ACKNOWLEDGMENTS

The authors thank Mrs. Cornelia Steinberg for performing the elemental analyses. They are also grateful for helpful discussions with Meret Leonie Betz and Dr. Vitaly Raev, IOT, and Dr. Detlef Loffhagen at INP, Greifswald. Tristan Winzer and Jan Benedikt acknowledge funding from the DFG, project BE4349/7-1. Lars Bröcker and Claus-Peter Klages acknowledge funding from the DFG, too, project KL 1096-38-1. Open Access funding enabled and organized by Projekt DEAL.

## DATA AVAILABILITY STATEMENT

The data that support the findings of this study are available from the corresponding author upon reasonable request.

## ORCID

Lars Bröcker  <http://orcid.org/0000-0002-7291-9265>

Jan Benedikt  <https://orcid.org/0000-0002-8954-1908>

Claus-Peter Klages  <https://orcid.org/0000-0001-5678-5845>

## REFERENCES

- [1] L. Bröcker, G. S. Perlick, C.-P. Klages, *Plasma. Process. Polym.* **2020**, *17*, 2000129.
- [2] M. K. Murphy, J. L. Beauchamp, *J. Am. Chem. Soc.* **1977**, *99*, 2085.
- [3] U. Weidner, A. Schweig, *Angew. Chem.* **1972**, *84*, 167.
- [4] L. Szepes, T. Baer, *J. Am. Chem. Soc.* **1984**, *106*, 273.
- [5] D. Henneberg, Silane, trimethyl-2-propenyl, Mass spectrum (electron ionization), <https://webbook.nist.gov/cgi/cbook.cgi?ID=C762721&Units=SI&Mask=200#copyright> (accessed: March 2023).
- [6] B. Chiavarino, M. E. Crestoni, S. Fornarini, *Organometallics* **2000**, *19*, 844.
- [7] R. N. Stillwell, D. I. Carroll, J. G. Nowlin, E. C. Horning, *Anal. Chem.* **1983**, *55*, 1313.
- [8] A. Kramida, Y. Ralchenko, J. Reader, Atomic Spectra Database, NIST Standard Reference Database 78, Version 5.10, <https://physics.nist.gov/asd> (accessed: March 2023).
- [9] U. Kogelschatz, *J. Opt. Technol.* **2012**, *79*, 484.
- [10] E. D. Palik, *Handbook of Optical Constants of Solids*, Vol. 2, Academic Press, Boston **1991**.
- [11] S. Große-Kreul, S. Hübner, S. Schneider, D. Ellerweg, A. von Keudell, S. Matejčík, J. Benedikt, *Plasma Sources Sci. Technol.* **2015**, *24*, 044008.
- [12] S. Murahashi, S. Nozakura, M. Sumi, *Stereoregular Polym.* **1958**, *32*, 670.
- [13] P. J. Elving, I. M. Kolthoff, *Chemical Analysis*, 41, John Wiley & Sons Inc, New York **1974**.
- [14] G. Socrates, *Infrared and Raman Characteristic Group Frequencies*, John Wiley & Sons, Chichester **2001**.
- [15] U. G. Stolberg, H. P. Fritz, *Z. anorg. allg. Chemie.* **1964**, *330*, 1.
- [16] N. Inagaki, H. Kobayashi, K. Shimohira, *Polym. Bull.* **1984**, *11*, 29.
- [17] J. L. C. Fonseca, D. C. Apperley, J. P. S. Badyal, *Chem. Mater.* **1992**, *4*, 1271.
- [18] J. E. Drake, B. M. Glavinčevski, C. Wong, *J. Inorg. Nucl. Chem.* **1980**, *42*, 175.
- [19] J. Z. Dávalos, T. Baer, *J. Phys. Chem. A* **2006**, *110*, 8572.
- [20] M. R. Alexander, F. R. Jones, R. D. Short, *Plasma Polym.* **1997**, *2*, 277.
- [21] C. Q. Jiao, C. A. DeJoseph Jr., A. Garscadden, *J. Vac. Sci. Technol., A* **2005**, *23*, 1295.
- [22] L. Klevan, B. Munson, *Int. J. Mass Spectrom.* **1974**, *13*, 261.
- [23] A. E. D. Heylen, *J. Sci. Instrum.* **1960**, *37*, 251.
- [24] A. E. D. Heylen, *J. Phys. D: Appl. Phys.* **1970**, *3*, 789.
- [25] A. E. D. Heylen, *Int. J. Electron.* **1971**, *30*, 121.
- [26] M. Yamane, *J. Phys. Soc. Jpn.* **1960**, *15*, 1076.
- [27] D. Loffhagen, M. M. Becker, A. K. Czerny, C.-P. Klages, *Plasma Chem. Plasma Process.* **2021**, *41*, 289.
- [28] V. I. Volodina, A. I. Tarasov, S. S. Spasskii, *Russ. Chem. Rev.* **1970**, *39*, 140.
- [29] D. Mikulášová, A. Hrivik, *Chem. Zvesti* **1957**, *11*, 641.
- [30] E. T. Denisov, *Russ. Chem. Bull.* **1999**, *48*, 442.
- [31] A. V. Topchiev, N. S. Nametkin, C. Hsiao-p'ei, S. G. Durgar'yan, V. I. Zav'yalov, *Org. Biomol. Chem.* **1963**, *2*, 269.
- [32] G. Natta, G. Mazzanti, P. Longi, F. Bernardini, *J. Polym. Sci.* **1958**, *31*, 181.
- [33] R. Zeigler, L. Resconi, G. Balbontin, G. Guerra, V. Venditto, C. De Rosa, *Polymer* **1994**, *35*, 4648.
- [34] S. Habaue, H. Baraki, Y. Okamoto, *Macromol. Chem. Phys.* **1998**, *199*, 2211.
- [35] G. Hagen, H. Mayr, *J. Am. Chem. Soc.* **1991**, *113*, 4954.
- [36] S. Aoshima, S. Kanaoka, *Chem. Rev.* **2009**, *109*, 5245.
- [37] N. R. Ball-Jones, A. A. Cobo, B. M. Armstrong, B. Wigman, J. C. Fettinger, J. E. Hein, A. K. Franz, *J. Am. Chem. Soc.* **2022**, *12*, 3524.
- [38] L. H. Sommer, L. J. Tyler, F. C. Whitmore, *J. Am. Chem. Soc.* **1948**, *70*, 2872.
- [39] A. Gandini, H. Cheradame, *Cationic Polymerization*, Springer Verlag, Berlin **1980**.
- [40] A. Tsikritea, J. A. Diprose, T. P. Softley, B. R. Heazlewood, *J. Chem. Phys.* **2022**, *157*, 060901.
- [41] Chemicalize, Calculate properties instantly, search chemical data, and draw molecules online, <https://chemicalize.com> (accessed: August 2023).
- [42] J. Nagy, S. Ferenczi-Gresz, V. F. Mironov, *Z. Anorg. Allg. Chem.* **1966**, *37*, 191.
- [43] M. Meot-Ner, L. W. Sieck, M. S. El-Shall, G. M. Daly, *J. Am. Chem. Soc.* **1995**, *117*, 7737.
- [44] Y. B. Pithawalla, M. Meot-Ner, J. Gao, M. Samy El-Shall, *J. Am. Chem. A* **2001**, *105*, 3908.
- [45] M. S. El-Shall, *Acc. Chem. Res.* **2008**, *41*, 783.
- [46] E. I. Izgrordina, M. L. Coote, *Chem. Phys.* **2006**, *324*, 96.
- [47] M. Samy El-Shall, A. Bahta, H. Rabeony, H. Reiss, *J. Chem. Phys.* **1987**, *87*, 1329.
- [48] Y. P. Raizer, *Gas Discharge Physics*, Springer Verlag, Berlin **1997**.
- [49] J. Cyriac, T. Pradeep, H. Kang, R. Souda, R. G. Cooks, *Chem. Rev.* **2012**, *112*, 5356.
- [50] J. Ghosh, R. G. Cooks, *TrAC* **2023**, *161*, 117010.
- [51] A. Khachatourian, H.-K. Chan, A. J. Stace, E. Bichoutskaia, *J. Chem. Phys.* **2014**, *140*, 074107.
- [52] P.-I. Wang, Z. Wu, T.-M. Lu, L. V. Interrante, *J. Electrochem. Soc.* **2006**, *153*, G267.

- [53] L. F. Thompson, K. G. Mayhan, *J. Appl. Polym. Sci.* **1972**, *16*, 2317.
- [54] R. K. Bose, S. Nejati, D. R. Stufflet, K. K. S. Lau, *Macromolecules* **2012**, *45*, 6915.
- [55] Y. Gao, B. Cole, W. E. Tenhaeff, *Macromol. Mater. Eng.* **2018**, *303*, 1700425.
- [56] A. M. Coclite, K. K. Gleason, *Plasma Process. Polym.* **2012**, *9*, 425.
- [57] K. K. S. Lau, K. K. Gleason, *Macromolecules* **2006**, *39*, 3695.
- [58] C.-P. Klages, K. Höpfner, N. Kläke, R. Thyen, *Plasmas Polym.* **2000**, *5*, 79.
- [59] J. Friedrich, *Plasma Process. Polym.* **2011**, *8*, 783.
- [60] T. Dufour, *Polymers* **2023**, *15*, 3607.
- [61] A. M. Wróbel, A. Walkiewicz-Pietrzykowska, J. E. Klemberg-Sapieha, Y. Hatanaka, T. Aoki, Y. Nakanishi, *J. Appl. Polym. Sci.* **2002**, *86*, 1445.
- [62] G. Odian, *Principles of Polymerization*, 4th ed., John Wiley & Sons, Hoboken **2004**.
- [63] L. Birladeanu, *J. Chem. Educ.* **2000**, *77*, 858.
- [64] G. Ferraris, C. Corno, A. Priola, S. Cesca, *Macromolecules* **1977**, *10*, 188.
- [65] L. Albers, S. Rathjen, J. Baumgartner, C. Marschner, T. Müller, *J. Am. Chem. Soc.* **2016**, *138*, 6886.
- [66] Z. A. Talib, S. Kurosawa, B. Atthoff, H. Aizawa, K. Kashima, T. Hirokawa, Y. Yoshimi, M. Yoshimoto, T. Hirotsu, J. Miyake, J. Hilborn, *J. Photopolym. Sci. Technol.* **2001**, *14*, 129.
- [67] A. R. Westwood, *Eur. Polym. J.* **1971**, *7*, 363.

**How to cite this article:** L. Bröcker, T. Winzer, N. Steppan, J. Benedikt, C.-P. Klages, *Plasma Process. Polym.* **2023**, e2300177.  
<https://doi.org/10.1002/ppap.202300177>